ACS APPLIED NANO MATERIALS

Article

Cite This: ACS Appl. Nano Mater. 2020, 3, 830−841

www.acsanm.org

p-Type Epitaxial Graphene on Cubic Silicon Carbide on Silicon for Integrated Silicon Technologies

Aiswarya Pradeepkumar,[†] Mojtaba Amjadipour,[†] Neeraj Mishra,[†] Chang Liu,[‡,§] Michael S. Fuhrer,[‡,§] Avi Bendavid,[∥] Fabio Isa,[∥] Marcin Zielinski,[⊥] Hansika I. Sirikumara,[#] Thushari Jayasekara,[#] D. Kurt Gaskill,[▽,○] and Francesca Iacopi*[,†,§]

[†]Faculty of Engineering and IT, University of Technology Sydney, Sydney, New South Wales 2007, Australia

[‡]School of Physics & Astronomy, Monash University, Melbourne, Victoria 3800, Australia

[§]ARC Centre of Excellence in Future Low-Energy Electronics Technologies, Melbourne, Victoria 3800, Australia

[∥]CSIRO Manufacturing, 36 Bradfield Road, Lindfield, New South Wales 2070, Australia

[⊥]NovaSiC, Savoie Technolac, Arche Bât. 4, BP 267, 73375 Cedex Le Bourget du Lac, France

[#]Department of Physics, Southern Illinois University, Carbondale, Illinois 62901, United States

[▽]US Naval Research Laboratory, Washington, D.C. 20375, United States

Supporting Information

ABSTRACT: The synthesis of graphene on cubic silicon carbide on silicon pseudosubstrates draws enormous interest due to the potential integration of the 2D material with the well-established silicon technology and processing. However, the control of transport properties over large scales on this platform, essential for integrated electronics and photonics applications, has lagged behind so far, due to limitations such as 3C-SiC/Si interface instability and nonuniform graphene coverage. We address these issues by obtaining an epitaxial graphene (EG) onto 3C-SiC on a highly resistive silicon substrate using an alloy-mediated, solid-source graphene synthesis. We report the transport properties of EG grown over large areas directly on 3C-SiC(100) and 3C-SiC(111) substrates, and we present the corresponding physical models. We observe that the carrier transport of EG/3C-SiC is dominated by the graphene−substrate interaction rather than the EG grain size, sharing the same conductivity and same inverse power law as EG on 4H- or 6H-SiC(0001) substrates—although the grain sizes for the latter are vastly different. In addition, we show that the induced oxidation/silicates at the EG/3C-SiC interface generate a p-type charge in this graphene, particularly high for the EG/3C-SiC(001). When silicates are at the interface, the presence of a buffer layer in the EG/3C-SiC(111) system is found to reduce somewhat the charge transfer. This work also indicates that a renewed focus on the understanding and engineering of the EG interfaces could very well enable the long sought-after graphene-based electronics and photonics integrated on silicon.

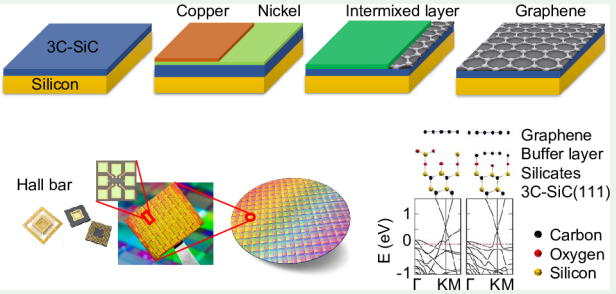

KEYWORDS: *epitaxial graphene, graphene/3C-SiC interface, substrate interaction, mobility, buffer layer, intercalation*

INTRODUCTION

Graphene has been extensively investigated over the past decade owing to its anticipated outstanding properties such as exceptional carrier mobility and room temperature ballistic transport.[1−4] The epitaxial growth of graphene on hexagonal (4H- and 6H-) silicon carbide (SiC) wafers has progressed substantially in both quality and process reliability.[3−15] However, when considering cost and wafer scaling challenges of bulk SiC wafers, as well as the relative immaturity of the SiC device technology vis-à-vis the well-established Si-based processing technologies, there is compelling interest to obtain epitaxial graphene (EG) also on silicon wafers for advancing a much wider range of integrated technologies such as integrated electronics and photonics. EG on silicon wafers have been pursued mainly using two different pseudosubstrates: one, a thin film of germanium,[16−18] and the other, a thin film of cubic silicon carbide (3C-SiC).[19−27] Table 1 shows a summary of attempts made toward the growth and electrical characterization of EG on Si wafers.

Although the growth of EG on Si wafers has been pursued in the past—using either thin films of 3C-SiC[19,21−27] or germanium,[16−18] the charge transport behavior of the obtained EG has not been thoroughly assessed over areas large enough to be relevant for semiconductor fabrication. Kang et al.[24] reported room temperature transport properties of few-layer graphene (FLG) grown via thermal decomposition on 3C-

Received: November 28, 2019
Accepted: December 11, 2019
Published: December 11, 2019

DOI: 10.1021/acsanm.9b02349
ACS Appl. Nano Mater. 2020, 3, 830−841

Table 1. Summary of Attempts to the Growth and the Transport Characterization of Epitaxial Graphene on Si Wafers at Room Temperature

epitaxial graphene		transport properties at 300 K					
substrate	growth process	n/p[a]	N[b] (cm^{-2})	μ[c] ($cm^2\ V^{-1}\ s^{-1}$)	R_{sh}[d] ($\Omega\ \square^{-1}$)	measurement technique	ref
3C-SiC(111)/n-Si(111)	thermal decom.	n	1.8×10^{13}			ARPES	21
(1) 3C-SiC(111)/p-Si(111), (2) 3C-SiC(111)/p-Si(110)	thermal decom.	n			(1) 17 k, (2) 90 k	top-gate FET, transmission line model (TLM)	23
3C-SiC(110)/Si(110)	thermal decom.	n	$0.6–3.4 \times 10^{11}$	430–6200	2.8–215 k	FLG back-gated FET	24
3C-SiC(111)/Si(111)	thermal decom.	(1) n, (2) n/p	6×10^{11}	(1) 950, (2) 175 (n), (2) 285 (h)	(1) 6 k	(1) noncontact Hall microwave method, (2) FET	22
3C-SiC(100)/Si(100), 3C-SiC(111)/Si(111)	CVD				3.5–50 k	Hg probe and c-TLM	19
device size Ge(100) islands/Si(100)	(1) CVD,[e] (2) MBE[f]	p	(1) 3×10^{13}, (2) 10^{12}	(1) 600 ± 300, (2) 1200 ± 400		4-point STM-FET	16
H-Ge(110)/Si(110)	CVD—(1), single cryst., (2) poly cryst.		3×10^{11}	(1) 10 620, (2) 2570	(1) 2–5 k, (2) 6–12 k	back-gated GFET on transferred graphene to SiO_2/Si	17
H-intercalated Ge(100)/Si(100)	CVD		(1) 6.8×10^{12}, (2) 9.2×10^{12}	(1) 950–1050, (2) 470–520		(1) before H-intercalation, (2) after H-intercalation	18

[a]Electrons/holes. [b]Sheet carrier concentration. [c]Mobility. [d]Sheet resistance. [e]Chemical vapor deposition. [f]Molecular beam epitaxy.

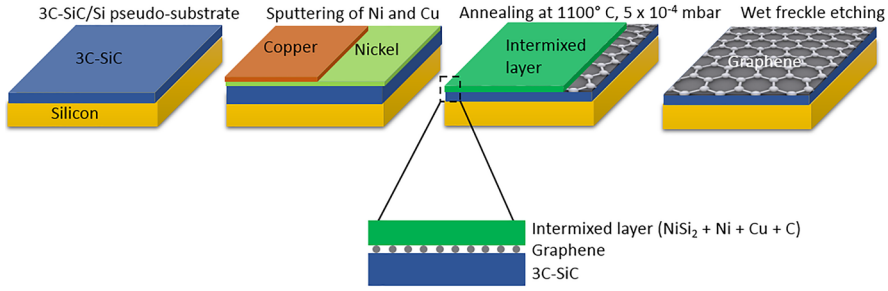

Figure 1. Schematic of the process steps for the alloy-mediated synthesis of graphene on the 3C-SiC/Si substrate.[20]

SiC(110) substrate using a back-gated field-effect transistor (FET); however, the results are complicated by the presence of a large amount of gate-leakage current. Moon et al.[22] and Lee et al.[17] also reported the room temperature transport properties of graphene on Si via intermediate 3C-SiC and H-terminated Ge layers, respectively. However, their measurements were performed, in the first case, using a noncontact Hall microwave-based (Lehighton) method, which is an unconventional and not benchmarked method, and in the second case, on EG only after it was transferred onto SiO_2/Si substrates—which, as we will show, is not representative of the electronic properties of the EG on the original substrate. Further to that, Debrowski et al.[16] have reported the electrical properties in FET configuration for the graphene grown on μm^2 size Ge(100) islands predeposited on Si(100) substrate. Evaluations of transport properties from FET measurements are geometry and electrostatics dependent and are affected by the substrate.[28] This type of transport measurements approach does not allow a thorough investigation of the scattering mechanisms. Temperature-dependent Hall effect measurements are required in order to provide the full information on the carrier transport in epitaxial graphene.

In this work, we use epitaxial 3C-SiC films grown on silicon wafers as pseudosubstrates for epitaxial graphene growth. As we had previously reported, the major historical limitations in using a 3C-SiC/Si substrate for graphene growth have been not only the difficulty to achieve continuous graphene coverage (mono- or multilayer) on the substrate[29] but also the instability of the 3C-SiC/Si heterojunction, hampering a reliable electrical characterization of the EG.[30,31] Note that these limiting factors have not been effectively addressed by the prior attempts reported in Table 1.

In this work, we are able to obtain continuous wafer-scale graphene coverage as well as overcome the parallel conduction issue by using a Ni/Cu alloy-mediated EG synthesis onto a highly resistive 3C-SiC grown on high-resistivity silicon substrates. The alloy-mediated approach enables a consistent EG coverage over large areas despite the highly defective heteroepitaxial 3C-SiC surface thanks to liquid-phase epitaxial growth conditions,[20] as opposed to the more conventional EG synthesis by thermal decomposition of the 3C-SiC.[21−27] The highly resistive silicon substrate, coupled with the high resistivity 3C-SiC, is essential to ensure a thorough electrical insulation of the EG from the substrate and enable the transport measurements of EG.[30] Room temperature van der Pauw (vdP) Hall effect measurements indicate p-type graphene on the 3C-SiC/Si pseudosubstrate unlike the typically n-type epitaxial graphene synthesized via thermal decomposition of 3C-SiC.[21,23−25,27,32] The temperature-dependent sheet resistance measurement confirms that the EG is electrically isolated from its underlying substrate system. Using Hall effect measurements, X-ray photoelectron spectroscopy (XPS), as well as density functional theory (DFT) calculations we demonstrate that the carrier transport in EG is determined by the strong interaction with its substrate, which contains interface silicates due to the alloy-mediated synthesis. Furthermore, our results imply that the transport properties of the alloy-mediated EG on 3C-SiC are independent of the

DOI: 10.1021/acsanm.9b02349
ACS Appl. Nano Mater. 2020, 3, 830−841

Table 2. Raman Mapping Characteristics at 300 K, for EG on 3C-SiC/Si of Both (100) and (111) Orientations Showing Grain Sizes Calculated from Intensity Ratios of D and G Bands, Peak Positions of G and 2D, and fwhm of G and 2D Bands[a]

			peak positions (cm^{-1})		fwhm (cm^{-1})	
sample	I_D/I_G	L_a[b] (nm)	G	2D	G	2D
			EG/3C-SiC(100)			
sample 1	0.24 ± 0.03	80 ± 10	1582.4 ± 0.1	2698.6 ± 0.1	26.3 ± 0.4	45.2 ± 0.3
sample 2	0.22 ± 0.03	87 ± 10	1582.5 ± 0.1	2699.2 ± 0.1	25.5 ± 0.5	45.3 ± 0.4
sample 3	0.22 ± 0.02	87 ± 10	1576.4 ± 0.3	2708.8 ± 0.3	27.9 ± 0.3	51.2 ± 0.2
			EG/3C-SiC(111)			
sample 1	0.22 ± 0.02	87 ± 10	1577.7 ± 0.2	2709.7 ± 0.2	27.0 ± 0.5	56.3 ± 0.5
sample 2	0.24 ± 0.02	80 ± 10	1581.3 ± 0.1	2698.0 ± 0.1	28.2 ± 0.3	49.2 ± 0.3
sample 3	0.34 ± 0.01	56 ± 10	1582.0 ± 0.1	2698.0 ± 0.1	27.2 ± 0.4	46.6 ± 0.3
sample 4	0.35 ± 0.01	55 ± 10	1582.4 ± 0.1	2696.7 ± 0.3	27.1 ± 0.4	55.8 ± 0.6

[a]Error bars correspond to the standard deviation of the measured values over an area of 30 × 30 μm^2. [b]Estimated grain size.

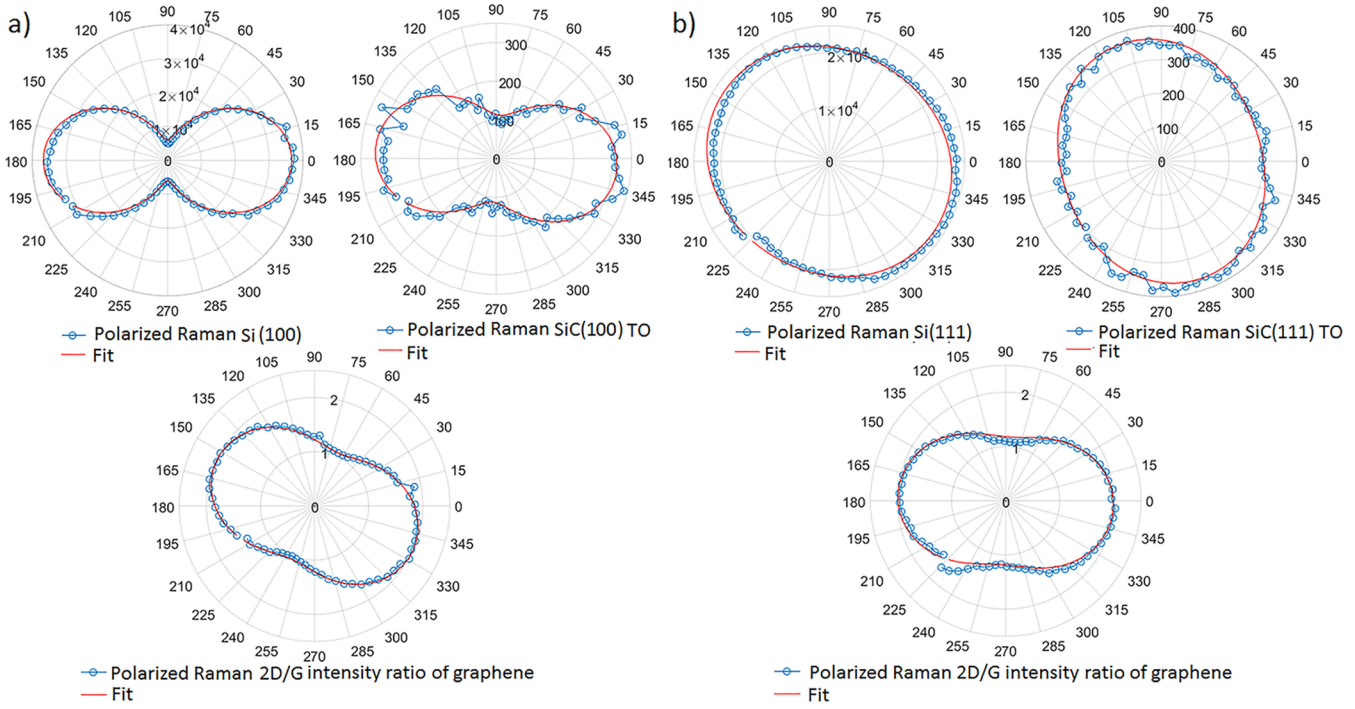

Figure 2. Polar plots of Si peak intensity, 3C-SiC TO peak intensity, and the ratio of the 2D to G peak intensity as a function of the relative angle (β) between the polarizations of the analyzer and incident laser, for (a) EG/3C-SiC(100); (b) EG/3C-SiC(111).

number of graphene layers as well as the domain sizes in the observed regime.

RESULTS AND DISCUSSION

The EG was obtained via a solid-source, Ni/Cu alloy-mediated method at ∼1100 °C below 5 × 10^{-4} mbar pressure as described by Mishra et al.[20] (see Figure 1; refer to the Materials and Methods section for more details on sample preparation and characterization tools). The EG samples have typically a root-mean-square roughness ∼9 nm, about 2-fold larger than the 3C−SiC/Si which is ∼4 nm.[20] Details on the number of graphene layers are provided in the X-ray Photoelectron Spectroscopy section of this Article.

Raman Characterization. Figure S1 shows the example maps of the Raman intensity ratio of D to G peak (I_D/I_G), 2D to G peak (I_{2D}/I_G), G position, 2D position, G full width half-maximum (fwhm), and 2D fwhm of the epitaxial graphene grown on 3C-SiC(100) and 3C-SiC(111) substrates. The maps show only a small range of variations across the measured region (quoted in Table 2) which indicates the uniformity of the graphene samples. Table 2 summarizes the Raman intensity ratios I_D/I_G and I_{2D}/I_G, positions of the G and 2D bands, and fwhm of the G and 2D bands for the selected EG samples. Figure S2 shows the average Raman spectra of the selected EG samples (across 30 μm × 30 μm area) from Table 2 indicating the SiC LO, D, G, and 2D Raman bands. I_D/I_G mapping ratios of the samples range between 0.22 (±0.03) and 0.35 (±0.01) (Table 2). We estimated the average graphene grain sizes for all the EG samples using the I_D/I_G[33] ratios. The grain sizes of the graphene samples range from 55 to 87 (±10) nm. Figure S3 shows the presence of in-plane modes indicative of turbostratic stacking of the graphene layers.[34] In addition, the 2D fwhm values given in Table 2 also indicate a turbostratic nature of multilayer graphene according to Malard et al.[35] (45−60 cm^{-1}). Turbostratic stacking has also been observed by Escobedo-Cousin et al. for the few-layer graphene formed by solid phase growth on the Si- or C-face of the bulk SiC.[9]

DOI: 10.1021/acsanm.9b02349
ACS Appl. Nano Mater. 2020, 3, 830−841

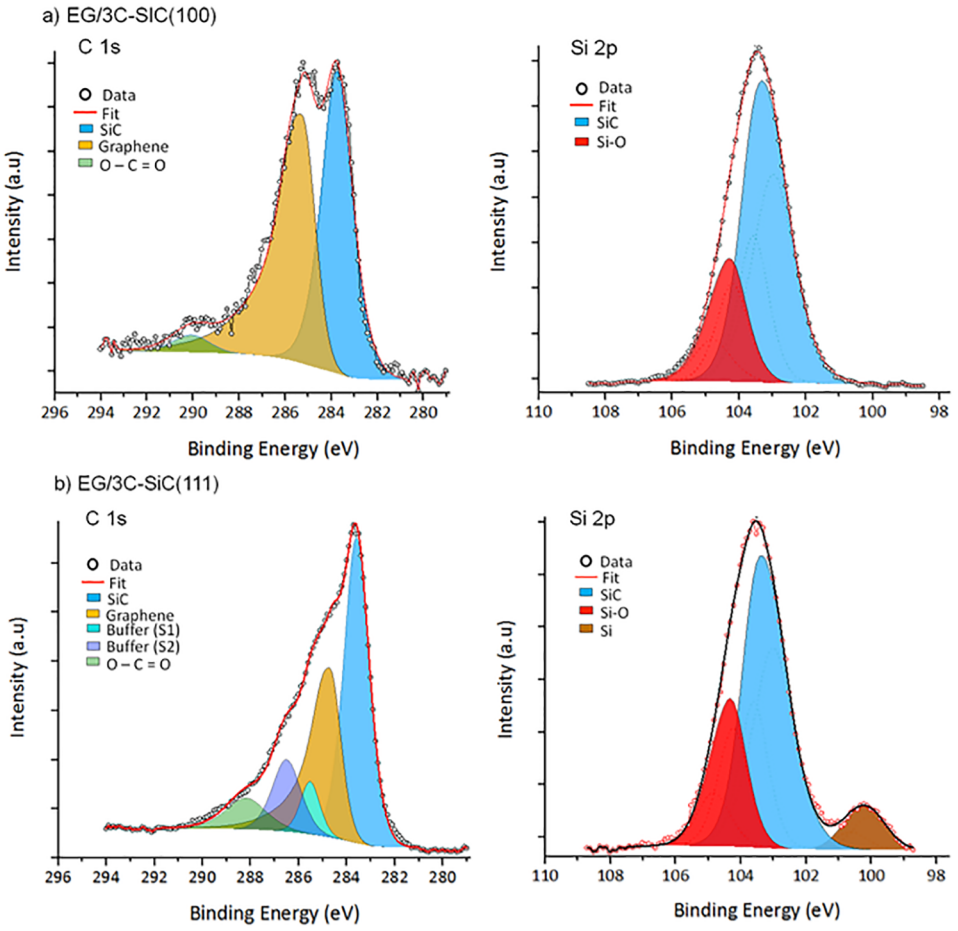

Figure 3. XPS C 1s and Si 2p core-level spectrum for (a) EG/3C-SiC(100) (sample 3 in Table 2) and (b) EG/3C-SiC(111) (sample 1 in Table 2).

The complexity of the 3C-SiC and Si interface is known to give rise to a range of defects,[36] yet polarized Raman data imply that the graphene is epitaxial with respect to the pseudosubstrate and hence justify describing it as epitaxial graphene. Figure 2 shows polar plots of the Raman Si peak, 3C-SiC TO peak,[37] and the graphene[38] 2D to G peak intensity ratio as a function of the relative angle (β) between the light polarization of the analyzer and incident laser, measured on single spots (see Figure S4 for additional plots taken on 2 other sample spots) for EG/3C-SiC(100) and EG/3C-SiC(111). The results show that the polarized Raman intensities for both the 3C-SiC and the EG have a preferential dependence on each other and with respect to the Si implying an epitaxial relationship among the triad. This is easily seen in Figure 2a where the preferred polarization angle of 3C-SiC with respect to the Si(100) substrate is about $-5 \pm 2°$ and that the EG polarization is about $-22 \pm 2°$ with respect to the Si(100). Differently, the Raman peak intensity for Si(111) and 3C-SiC(111) is almost independent of the polarization angle β[39] as shown in Figure 2b. Even though it is not possible to use the Si(111) and 3C-SiC(111) for crystallographic references, the maximum of the EG 2D to G Raman intensity ratio is consistent within 3° all over the measured sample spots. We attribute the variation in crystallographic orientation of the EG on Si(100) and Si(111) to the turbostratic nature of the EG and differences in interface structure (see the X-ray Photoelectron Spectroscopy section below). The plots in Figure 2 clearly indicate that the graphene synthesized using the alloy-mediated approach exhibits an epitaxial relation with the highly defective 3C-SiC pseudosubstrate. We note that the angle of rotation of the alloy-mediated graphene with the pseudosubstrate is smaller than that of the graphene synthesized on bulk SiC,[27,40] which is also likely related to the turbostratic nature of the EG.

X-ray Photoelectron Spectroscopy. Figure 3 shows the XPS C 1s and Si 2p spectra of EG3C-SiC(100) and EG/3C-SiC(111). A combination of Gaussian and Lorentzian line shapes (Voigt) is used to fit the curves. The background is subtracted using the Shirley procedure.[41] For EG/3C-SiC(100), three peaks are used to fit the C 1s spectra, which corresponds to SiC (~283.7 eV), graphene (~285.2 eV), and O—C═O (~290 eV).[9] The EG/3C-SiC(111) C 1s spectrum is different as it shows photoelectron peaks at ~283.6 eV (SiC), ~284.7 eV (graphene), and O—C═O (~288.2 eV) and buffer layer components at 285.5 eV (S1) and 286.4 eV (S2). The presence of a buffer layer in EG/SiC(111) has also been previously reported in the literature.[21,27,42] The graphene layer thicknesses are estimated from the C 1s data[43] (see the Supporting Information (SI), section 2, for details). The overall variation of EG thickness across different samples ranges from 3 to 7 layers. Note that since the EG/SiC/Si shows turbostratic stacking, a weak interaction is expected among the layers so that the multilayer graphene is expected to be electrically equivalent to a monolayer.[35]

The Si 2p spectra are fitted with Si $2p_{3/2}$ and Si $2p_{1/2}$ spin–orbit doublets with 0.6 eV splitting: Si–C (~101.3), Si–O

DOI: 10.1021/acsanm.9b02349
ACS Appl. Nano Mater. 2020, 3, 830–841

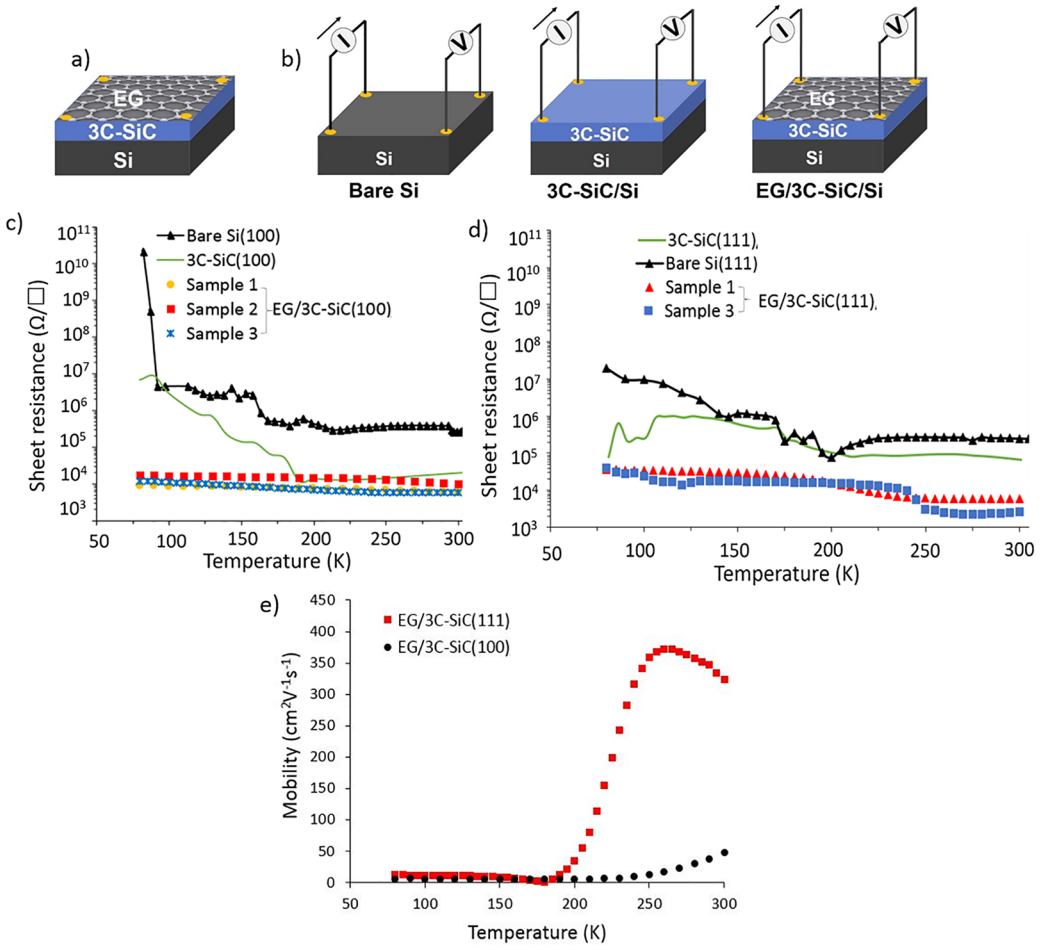

Figure 4. (a) van der Pauw geometry with four-point InSn contacts. (b) Schematics of vdP sheet resistance measurements on bare-Si, 3C-SiC/Si, and EG/3C-SiC/Si. Temperature-dependent sheet resistance of (c) EG/3C-SiC(100), 3C-SiC/Si(100), and bare-Si(100); (d) EG/3C-SiC(111), 3C-SiC/Si(111), and bare Si(111) in the range between 80 and 300 K. (e) Mobility as a function of temperature in the range between 80 and 300 K for EG/3C-SiC(100) and EG/3C-SiC(111).

(~102.5), Si (~99); the peak positions are reported for Si $2p_{3/2}$. The Si 2p spectra of both EG/3C-SiC(100) and EG/3C-SiC(111) indicate Si−O bonds at ~102.5 eV. This signifies a considerable amount of top-substrate oxidation/silicates at the EG/3C-SiC interface—just underneath the graphene. In the case of 3C-SiC(111), the presence of stacking faults[36] promotes out-diffusion of silicon into the SiC, which is observed at ~100.2 eV in the XPS Si 2p of EG/3C-SiC(111). Note that neither the XPS survey spectrum (within the range between 850 and 960 eV[44,45]) nor the energy-dispersive X-ray spectroscopy (EDX) indicates the presence of metal (nickel or copper) or metal oxides in the graphene (see Figure S5 for EG on 3C-SiC(100) (sample 3) and 3C-SiC(111) (sample 1)).

Electrical Characterization. We investigated the room temperature transport properties of the EG samples synthesized on both 3C-SiC(100) and 3C-SiC(111) substrates using the van der Pauw configuration as shown in Figure 4a. The room temperature properties are summarized in Table 3.

The EG synthesized on 3C-SiC(100) shows p-type carriers with sheet carrier concentration in the range between ~1.5 and 3.3 (±0.2) × 10^{13} cm^{-2}, mobility in the range 30−84 (±2) cm^2 V^{-1} s^{-1}, and sheet resistance between 6 and 11 (±1) kΩ $\square^{-1}$ at 300 K. These values are in good agreement with results obtained using setup 2, an additional setup with cryogenic capabilities (see the Materials and Methods section for details).

Table 3. Hall Measured Transport Properties at 300 K[a]

sample	carrier type	sheet carrier concentration (±0.2) × 10^{13} cm^{-2}	mobility (±2) cm^2 V^{-1} s^{-1}	sheet resistance (±1) k Ω $\square^{-1}$
EG on 3C-SiC(100)				
sample 1	holes	1.5	63	6
sample 2	holes	1.0	84	11
sample 3	holes	3.3	30	6
EG on 3C-SiC(111)				
sample	carrier type	sheet carrier concentration (±0.2) × 10^{12} cm^{-2}	mobility (±2) cm^2 V^{-1} s^{-1}	sheet resistance (±1) k Ω $\square^{-1}$
sample 1	holes	3.3	330	6
sample 2	holes	4.6	144	9
sample 3	holes	7.0	305	2.5
sample 4	holes	3.3	330	6

[a]The errors represent the maximum variation of the values upon the current sweep from 1 to 10 μA.

As a comparison, the corresponding bare Si(100) substrate shows n-type conduction with sheet carrier concentration, mobility, and sheet resistance of 1.0 (±0.2) × 10^{10} cm^{-2}, 1300 (±10) cm^2 V^{-1} s^{-1}, and 500 (±3) kΩ $\square^{-1}$, respectively. The 3C-SiC grown on Si(100) also indicates electrons as charge

DOI: 10.1021/acsanm.9b02349
ACS Appl. Nano Mater. 2020, 3, 830−841

carriers and sheet carrier concentration of 2.0 (±0.2) × 10^{11} cm^{-2}, mobility of ~1700 (±10) cm^2 V^{-1} s^{-1}, and sheet resistance of ~20 (±1) kΩ $\square^{-1}$. The electron mobility of 3C-SiC(100) is in accordance with the expected values for 3C-SiC of thickness between 15 and 30 μm.[46]

Hall measurements at 300 K of the EG grown on the 3C-SiC(111) orientation also indicate p-type charges. The charge carriers in this EG show larger mobilities (144−330 (±2) cm^2 V^{-1} s^{-1}), on average about 5 times higher than those of the EG on 3C-SiC(100) substrates, with sheet carrier concentrations of the order of 10^{12} cm^{-2}, ~2−5 times smaller than EG on (100) oriented 3C-SiC/Si. The sheet resistances of the samples fall in the range between 2.5 and 10 kΩ $\square^{-1}$. Again, as a comparison, the bare Si(111) substrate shows p-type conduction with sheet carrier concentration, mobility, and sheet resistance of 7 (±0.2) × 10^{10} cm^{-2}, 340 (±10) cm^2 V^{-1} s^{-1}, and 270 (±10) kΩ $\square^{-1}$, respectively. The 3C-SiC(111) grown on Si(111) exhibits hole type conduction and has sheet carrier concentration of 4.0 (±0.2) × 10^{11} cm^{-2}, mobility of ~250 (±10) cm^2 V^{-1} s^{-1}, and sheet resistance of ~70 (±3) kΩ $\square^{-1}$. 3C-SiC/Si is usually unintentionally n-type doped, but in this case, we find a p-type 3C-SiC/Si, which is attributed to the dissuaded carrier inversion effect discussed by Pradeepkumar et al.[30] which is indicative of an unstable p−n heterojunction. Nevertheless, since the 3C-SiC and Si are highly resistive, this does not affect the isolation of graphene on the SiC/Si. Note that the mean free path[47] estimated from the mobility and sheet carrier concentration values from Table 3 for EG on both 3C-SiC(100) and 3C-SiC(111) are within a 3−10 nm range.

Further, Figure 4b schematically shows the configuration used for sheet resistance measurements; note that all permutations are used to extract the sheet resistance data. Figure 4c,d shows the temperature-dependent sheet resistance behavior for EG/3C-SiC/Si, 3C-SiC/Si, and the bare-Si substrates between 80 and 300 K for the (100) and (111) surfaces, respectively. The sheet resistance behavior of the EG samples can be clearly distinguished from that of the underlying 3C-SiC/Si and Si substrates by the weak temperature dependence (refer also to Figure S6 for sheet resistance measurements down to 4 K). The sheet resistance data versus temperature also point out that the EG is covering continuously the underlying SiC/Si system. When the coverage is not continuous, this can be easily recognized through the strange temperature dependence of sheet resistance in Figure S8a. Figure 4e shows temperature-dependent mobility of EG/3C-SiC(100) and EG/3C-SiC(111). The mobility of EG grown on 3C-SiC(100) surface has a weak temperature dependence, gradually increasing after 200 K attaining ~30 cm^2 V^{-1} s^{-1} at 300 K. The weak temperature dependence of mobility of EG/3C-SiC(100) may be due to the absence of a buffer layer, consistent with the previous report by Speck et al. for EG on SiC.[10] On the other hand, the mobility of EG/3C-SiC(111) shows a sharp increase after 200 K up to a value of ~375 cm^2 V^{-1} s^{-1} at 250 K and then a decrease until ~330 cm^2 V^{-1} s^{-1} at 300 K. The negative temperature dependence of mobility above 250 K for the EG/3C-SiC(111) may be related to the scattering process originating at the buffer layer—as reported for EG on 6H-SiC.[48]

Next, we compare the sheet carrier concentration and mobility values of the EG given in Table 3 with those of the EG grown on 4H- and 6H-SiC from Tedesco et al.[7] Figure 5 shows that the mobility and sheet carrier concentration of the EG on 3C-SiC(100) and 3C-SiC(111) follow a very similar

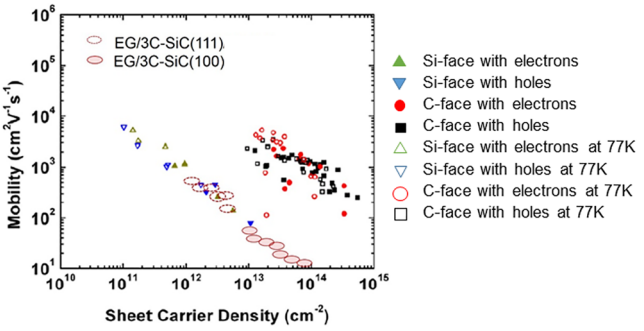

Figure 5. Mobility and sheet carrier density data of the EG on 3C-SiC/Si (Table 3) are here superimposed and remarkably in line with those of EG on the Si-face of bulk 4H- and 6H-SiC 16 × 16 mm^2 semi-insulating substrates at 300 and 77 K from Tedesco et al.[7] Reprinted from ref 7. Copyright 2009 AIP publishing.

power law dependence to those of EG grown on the Si-face of bulk 4H- and 6H-SiC wafers from Tedesco et al.[7] The inverse power law model has been reported as an intrinsic property of epitaxial graphene[7] and is also in agreement with additional reports of EG on SiC(0001).[49] We will elaborate further on the relevance of this model for this study.

First of all, the combined and deidentified mobility versus sheet carrier concentration data for EG on Si-face SiC from Tedesco et al.,[7] together with the values for the EG on 3C-SiC from this work, can be fitted as a whole with good confidence with the same power law, indicating a common conductivity of about ~3 ± 1 (e^2/h), value close to the expected minimum quantum conductivity of graphene—see Figure S7b. The general nature of the power law in Figure 5 also indicates that the tunability of the transport properties of epitaxial graphene is constrained; i.e., when the carrier concentration increases, the mobility has to decrease accordingly.

The power law trend exhibited in Figure 5 could be due to short-range weak disorder potentials dominating the carrier scattering process; then, one expects a conductivity independent of the carrier density, and then, the mobility would be inversely proportional to the sheet carrier concentration.[50] However, we note that the power law trend could also be explained by long-range scattering behavior[51,52] where the dopants are considered as the main scattering impurities. For this latter case, conductivity would be a constant,[52] and again, the mobility would be inversely proportional to the sheet carrier concentration. We note that the latter model would be consistent with interface interaction (i.e., the silicates) dominating the scattering process and, hence, the EG transport properties.[53]

The significant difference in the mobility range between the graphene grown on Si-face and C-face of hexagonal SiC wafers was reported as due to the distinct levels of graphene−substrate interactions on Si-face and C-face surface terminations by Norimatsu et al.[11] For the graphene on Si-terminated SiC(0001) surface, a strong covalent bond interaction of buffer layer with the substrate was reported, whereas the graphene on the C-face of SiC(0001) forms only a weak interaction with the substrate.[11,54] The significantly lower mobility values at higher sheet carrier concentrations of the EG on 3C-SiC(100) may imply that the graphene possesses much stronger substrate interaction than even the EG on Si-face of hexagonal SiC wafers. We had previously measured the substrate interaction of the EG on 3C-SiC(100), using the

DOI: 10.1021/acsanm.9b02349
ACS Appl. Nano Mater. 2020, 3, 830−841

double cantilever beam method (DCB).[55] This measurement has yielded an adhesion energy close to 6 J m^{-2}, which is ~3 times larger than the adhesion energy of the graphene to the Cu foils, PMMA, and SiO_2 (transferred), as measured with DCB.[55] The adhesion evaluation of EG on bulk SiC with the DCB is extremely challenging, and no corresponding value is found in the literature. An attempt to quantify the adhesion of the interface between the EG and the bulk SiC was made by Kim et al.,[56] based on the stress-delamination theory—which hence cannot be compared with the values from the double cantilever method, as the latter is based on a sandwiched configuration and pure opening mode.[57] Another attempt to measure the adhesion energy of EG on Si-face of SiC was made by Wells et al., who reported a value of ~3 J m^{-2}—estimated from the graphene pleat defects.[58] In the case of EG on 3C-SiC(111), even if the interface silicates are present, the mobility and carrier concentration values of EG are close to those on Si-face of SiC. This may indicate that EG on 3C-SiC(111) possesses similar adhesion energy as that of the EG on Si-face SiC.

The epitaxial graphene grown via thermal decomposition on hexagonal SiC or 3C-SiC/Si substrates is generally n-type doped.[12,13,59] The EG in this work shows a p-type conduction. It is well-known that the presence of electron affinitive oxygen at the interface attracts charge carriers from the graphene.[9,60] The charge transfer from EG into the oxides at the EG/3C-SiC interface is hence likely responsible for the p-type doping in this epitaxial graphene. Even though an equivalent amount of substrate oxidation is detected by the XPS in the case of EG/3C-SiC(111), the presence of buffer layer between graphene and 3C-SiC(111) may screen the substrate interaction of EG;[61−63] i.e., charge transfer from graphene to top-oxidized SiC could be reduced up to some extent by having a buffer layer between epitaxial graphene and the substrate. Consequently, we believe that the buffer layer screening is the reason behind the lower sheet carrier concentration and improved mobility of EG/3C-SiC(111) compared to the EG/3C-SiC(100) which does not possess a buffer layer. Although the carrier mobilities of the EG/3C-SiC/Si appear overall lower than those of EG grown on hexagonal SiC wafers,[7] the sheet resistance values are comparable. The sheet resistance of EG/3C-SiC(100) from this work varies from 10−30 kΩ $\square^{-1}$ at 4 K (Figure S6a) down to 6−11 k Ω $\square^{-1}$ at 300 K (Figure S6a and Table 3), and the sheet resistances of EG/3C-SiC(111) varies from ~100 kΩ $\square^{-1}$ at 4 K (Figure S6b) down to 2.5−10 kΩ $\square^{-1}$ at 300 K (Figure S6b and Table 3). Berger et al.[3] reported square resistances of 1.5 k to 225 kΩ $\square^{-1}$ at 4 K for patterned graphene films on SiC. Another work from the same research group[64] has reported, for EG on Si-face SiC, sheet resistance in the similar range which is ~1.5−4.2 kΩ $\square^{-1}$ at 300 K and ~2−7 kΩ $\square^{-1}$ at 4 K, respectively. This indicates that the EG grown on 3C-SiC/Si via the alloy-mediated approach has a sheet resistance/conductivity comparable to that of EG on SiC (0001) substrates. In addition, we note that the convergence to the same inverse power law trend observed in Figure 5 further confirms that all of the samples of EG/3C-SiC(100), EG/3C-SiC(111), as well as the EG on bulk SiC (Si−face) have roughly the same sheet resistance, which is close to the expected maximum quantum resistance for graphene (see also Figure S7a).

This may appear surprising as the grain sizes for EG on bulk SiC are at least 100 nm and upward,[14,65,66] whereas the estimated grain size for the EG/SiC/Si is significantly smaller (Table 2). We also observe from Table 2 that the grain sizes of both EG/3C-SiC(100) and EG/3C-SiC(111) are comparable, yet their mobilities differ by at least a factor of 5. Finally, we note that the estimated mean free path of the carriers in the EG/SiC/Si (3−10 nm) is much smaller than its grain size as assessed via Raman (Table 2). This all suggests that the grain sizes are not the determining factor in the transport properties of the graphene.

Finally, we also note that the variation of number of layers for the EG/SiC/Si samples does not affect the measured transport properties (see also the SI, section 3), which is expected for turbostratic stacking of graphene.[35]

To assess the effect of substrate interaction on the transport properties of graphene, we have used an atomistic model for EG on 3C SiC(111), 2 × 2 graphene cell on top of $\sqrt{3} \times \sqrt{3}$ *R* cos 30 SiC supercell. This model has been widely used for studying EG on 6H-SiC(0001).[60] Our first principle calculations for the EG/3C-SiC(111) show that an EG sample on top of a buffer layer with no silicates yields an n-type doped graphene (see Figure S9), similarly to the EG obtained through the more conventional thermal decomposition method on 6H-SiC(0001)[3,12,13,59] and ARPES-reported values of EG on 3C-SiC(111).[21,25,27] The alloy-mediated synthesis used in this work induces oxidation on the surface of the SiC layer as demonstrated by the XPS data. In the case no buffer layer was present (at 100% oxidation, 5 O atoms per unit cell), our calculations show p-type graphene due to charge transfer from the graphene to interfacial oxides (see Figure 6a). We propose that a similar charge transfer arises for the case of EG/3C-SiC(100), with no buffer. In the case of the EG/3C-SiC(111), where we observe a buffer layer with XPS, we have modified the calculation to reflect the presence of a buffer taking into account a 60% surface oxidation level. We find from these calculations that EG/3C-SiC(111) is also p-type,

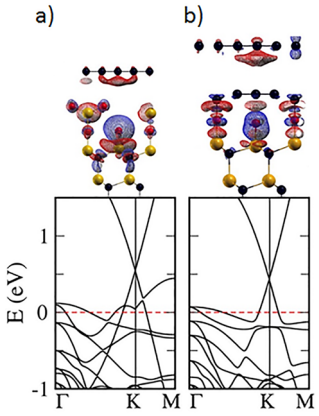

Figure 6. Electronic band structure for EG on 3C-SiC with top-substrate demonstrating the effect of substrate interaction on transport properties of epitaxial graphene. (a) Absence of buffer layer (at 100% oxidation) increases a charge transfer from graphene into the oxidized substrate with a Fermi level at 0.55 eV below the Dirac point, which can be linked to the case of EG/3C-SiC(100). (b) Presence of buffer layer (at 60% oxidation) between EG and substrate reduces the charge transfer from graphene giving Fermi level at 0.43 eV below the Dirac point (E_F closer to E_D), reflecting the case of EG/3C-SiC(111). Si, C, and O atoms are shown in yellow, black, and red spheres. The upper panels show the charge density plot. The blue color mesh represents electron accumulation, and the red color mesh indicates electron depletion.

DOI: 10.1021/acsanm.9b02349
ACS Appl. Nano Mater. 2020, 3, 830−841

Table 4. Hall Characteristics at 300 K before and after H-Intercalation of EG/3C-SiC(111) (Sample 4)

	EG on 3C-SiC(111)	
	before H-intercalation	after H-intercalation
carrier type	holes	holes
sheet carrier concentration (cm^{-2})	$3.3(\pm0.2) \times 10^{12}$	$2.8(\pm0.2) \times 10^{12}$
mobility ($cm^2\ V^{-1}\ s^{-1}$)	330(±2)	350(±2)
sheet resistance ($\Omega\ \square^{-1}$)	6k ± 1k	6k ± 1k

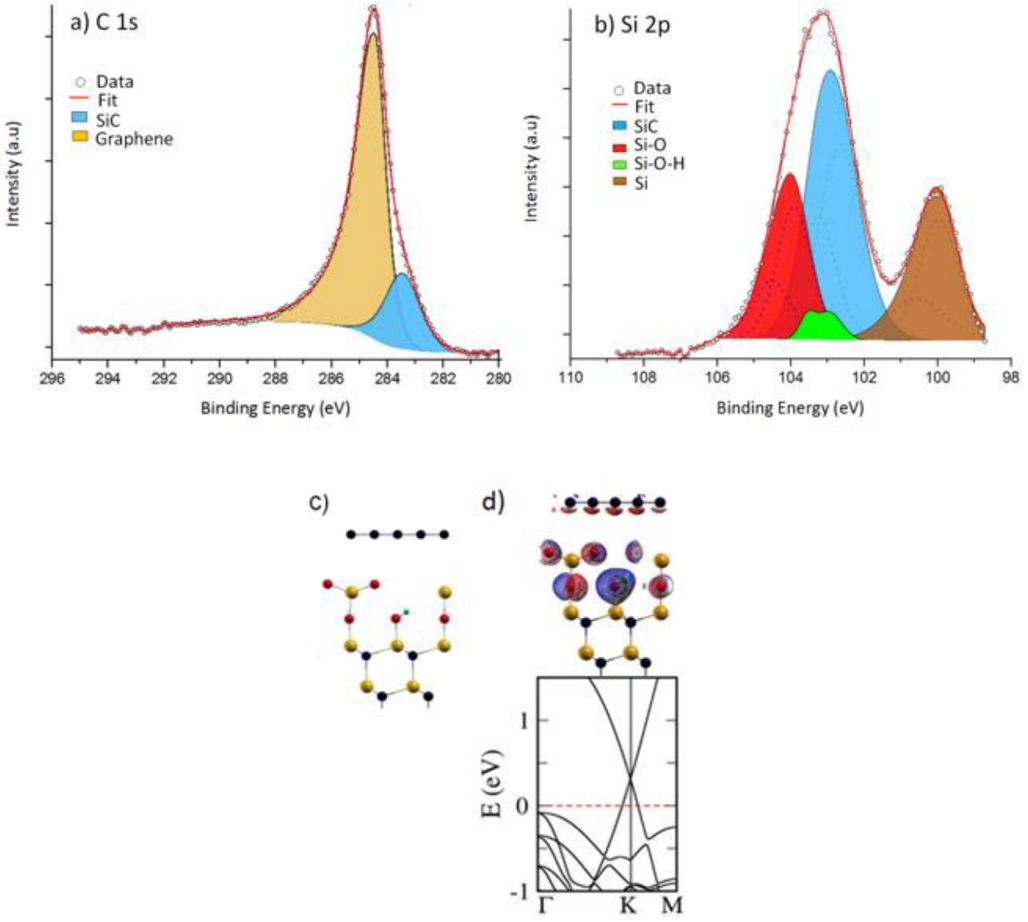

Figure 7. (a, b) XPS C 1s and Si 2p core-level spectrum for a selected EG/3C-SiC(111) (sample 4) after H-intercalation. (c, d) Schematic and electronic band structure for H-intercalated EG on top-oxidized substrate 3C-SiC(111) with Fermi level at 0.32 eV, below the Dirac point ($E_D - E_F$) indicating p-type conduction. The upper panel in part d shows the charge density plot. Si, C, O, and H atoms are shown in yellow, black, red, and green spheres. The blue mesh represents the electron accumulation, and the red mesh indicates electron depletion.

although its Fermi level is closer to the Dirac point as compared to the calculation for EG/3C-SiC(100) (see Figure 6b).

The electronic band structures in Figure 6a,b show Fermi level positions below the Dirac point at ∼0.55 and ∼0.43 eV, respectively. The p-type sheet carrier concentrations estimated from the Fermi levels[21] are $\sim 1.8 \times 10^{13}$ cm^{-2} in the first case, which can be related to that of the EG/SiC(100)/Si, and $\sim 1.1 \times 10^{13}$ cm^{-2}, ∼1.6 times smaller, in the second case which can be linked to the EG/3C-SiC(111)/Si. This trend is similar to the observed Hall transport properties reported in Table 3, and it supports that the difference observed in the transport properties of EG/3C-SiC(100) versus EG/3C-SiC(111) is attributed to the presence/absence of buffer layer resulting in a weaker/stronger EG−substrate interaction.

In an attempt to further reduce the substrate interaction on the transport properties of EG/3C-SiC(111), we performed H-intercalation. The intercalation was performed at conditions similar to Koch et al.[15] (see the Materials and Methods section for more details). Table 4 reports the Hall measured transport properties at 300 K for EG/3C-SiC(111) (sample 4) before and after the H-intercalation.

Mammadov et al.[12] and Sirikumara et al.[60] reported that H-intercalated EG on 3C-SiC(111) substrates shows n-type carriers, as passivation of dangling bonds with hydrogen modifies electronic density in graphene when graphene attracts charges from the passivated H atom. However, the observed extent of reduction in sheet carrier concentration after the H-intercalation of EG/3C-SiC(111) in Table 4 is only minor.

Figure 7a,b shows the C 1s and Si 2p spectra of the EG/3C-SiC(111) after H-intercalation.

C 1s spectra indicate that the H-intercalation process decouples the buffer layer from the substrate.[41,61] The Si 2p spectrum shows the presence of Si−O bonds (102.5 eV) and

DOI: 10.1021/acsanm.9b02349
ACS Appl. Nano Mater. 2020, 3, 830−841

an additional Si−O−H bond at 102 eV. We believe that the charge transport properties of the graphene even after decoupling the buffer layer did not show considerable improvement (Table 4) because the interface was still occupied by the silicates (Figure 7b), which dominates the charge transport in the EG. The effect of the H-intercalation on transport properties has also been analyzed with the help of DFT calculation (Figure 7c,d). The schematic shows that, after H-intercalation, the buffer layer in EG/3C-SiC(111) is decoupled, and the Fermi level for the EG is at 0.32 eV below the Dirac point. The estimated sheet carrier concentration is ~6 × 10^{12} cm^{-2}, whose points imply a 2-fold expected reduction in the sheet carrier concentration from the nonintercalated EG/3C-SiC(111) (~1.1 × 10^{13} cm^{-2}, Figure 6b).

CONCLUSIONS

Epitaxial graphene on 3C-SiC on silicon is of high technological relevance and has been pursued extensively over the past decade to allow for seamless integration with silicon technologies. Graphene on silicon could indeed extend the scope of silicon technologies to enable advanced electronics, including low-loss high-frequency active and passive devices, to on-chip nanophotonics and low-loss plasmonics. All of the aforementioned applications require a very detailed understanding and control of the transport properties of graphene on the silicon pseudosubstrate. However, the lack of large-scale graphene continuity over the 3C-SiC and an unstable 3C-SiC/Si heterointerface had limited adequate characterization and modeling of the electronic transport properties of EG on 3C-SiC on silicon wafers.

In this work, we overcome such issues and describe the transport properties of epitaxial graphene grown over large areas via an alloy-mediated graphitization approach on highly resistive 3C-SiC formed on high-resistivity silicon wafers and also show the corresponding density-functional theory models. Despite a defective substrate (3C-SiC/Si),[36] the polarized Raman measurements demonstrate that the graphene synthesized via the alloy-mediated approach maintains an epitaxial relationship with the substrate; hence, using the terminology epitaxial graphene is justified.

We find that the epitaxial graphene is strongly p-type doped as a result of the interaction with the substrate that comprises silicates generated at the EG/SiC interface by the alloy-mediated epitaxial synthesis, as opposed to the n-type doping found for EG from thermal decomposition of SiC. The estimated charge mean free path for the EG/3C-SiC/Si wafers ranges between 3 and 10 nm, which is a much smaller length than the estimated grain size of the EG. This further evidence indicates that in all cases the transport behavior of the EG on 3C-SiC/Si is dominated by the interaction with its substrate. The charge transport properties of the alloy-mediated EG are surprisingly close to those of EG on SiC, particularly, showing comparable sheet resistance values and the same inverse power model dependence of the EG sheet carrier concentration and mobility, although the grain sizes are different in both cases. The power law dependence further demonstrates that the carrier transport in EG is determined by the substrate interaction and is affected by the presence of silicates at the interface. The EG on 3C-SiC(111) has a buffer layer, whereas EG on 3C-SiC(100) lacks a buffer layer, consistent with the literature. DFT calculations are consistent with the carrier type and charge transfer from interfacial silicates. The number of layers is in the range between 3 and 7 for EG on both 3C-SiC(100) and 3C-SiC(111) and are turbostratic, in contrast with the EG formed by Si sublimation. The transport properties are independent of the number of layers which is consistent with turbostratic nature of the graphene.

The research group of de Heer reported that the multilayer EG with a silicate layer on top of the SiC enables the tunnelling process through the silicate/Schottky layer/barrier that could be utilized for the development of transistors.[67] In addition, Padilla et al. studied the tunability of graphene/metal-intercalated silicate/SiC and demonstrated the possibility for electronic band engineering based on the graphene/SiC interface.[68] The transport measurements of EG/3C-SiC indicate that engineering the interface is key to the control of the transport properties of the EG. We conclude that a renewed attention to more efficient intercalation processes could very well enable epitaxial graphene on silicon substrates for superior integrated functionalities ranging from nanoelectronics to nanophotonics.

MATERIALS AND METHODS

Sample Preparation: Synthesis of EG on Cubic Silicon Carbide on Silicon. We use unintentionally doped, NOVASiC 3C-SiC films with 500 nm thickness, epitaxially grown on 235 μm thick highly resistive (resistivity >10 kΩ cm) Si(100) as well as Si(111) substrates.[30] Prior to graphene growth, the 3C-SiC/Si substrate wafers are diced into 1.1 × 1.1 cm^2 coupons and cleaned in acetone and isopropanol. The alloy-mediated graphene growth was performed via a solid-source method using nickel and copper as catalysts and annealing at 1100 °C, 5 × 10^{-4} mbar as reported elsewhere.[20] After annealing, the samples undergo a wet Freckle (~20 h) etch to remove the metal residues and silicides. Subsequent characterizations are performed after the wet etch step.

Electrical Characterization. Four-point InSn ohmic contacts are soldered onto the EG/3C-SiC/Si samples and representative bare high-resistivity Si substrates and 3C-SiC/Si coupons. We measured the room temperature carrier concentration, carrier mobility, and sheet resistance by performing Hall effect measurements at a magnetic field of 0.55 T and the current range 1−10 μA using an Ecopia Hall effect measurement system, HMS-5300.[30] Transport measurements are performed on at least 10 samples each of EG/3C-SiC(100) and EG/3C-SiC(111) (selected samples are reported in Table 3). The errors represent the maximum variation of the values upon the current sweep. The temperature-dependent sheet resistance measurements of the graphene samples as well as the 3C-SiC and Si substrates are performed between 80 and 300 K using the Ecopia HMS-5300 system. Equivalent low-temperature sheet resistance measurements in the range between 4 and 300 K are also performed on selected samples using a Quantum Design physical property measurement system (PPMS) (referred to as setup 2) at Monash University. The source current is applied through a Keithley 2400 SourceMeter, which recorded the voltage simultaneously.

Raman Spectroscopy. Confocal Raman mapping at room temperature was performed using a Renishaw InVia spectrometer operating at 532 nm laser line using a 50× objective with a spot size of approximately 1 μm and incident power of 17 mW.[20] We used a silicon sample as reference (~520 cm^{-1}) for calibration. A 30 μm × 30 μm area is mapped using a 0.20 μm step size, and 0.1 s integration time at the center of each sample. The Raman D, G, and 2D bands of the graphene are examined, and the D to G band intensity ratio (I_D/I_G), G and 2D band peak positions, G, and 2D band fwhm were calculated by fitting the maps across the 30 μm × 30 μm area. The error values represent the standard deviation of the I_D/I_G ratios, measured at five different sites.

Polarized Raman Spectroscopy. Polarized Raman measurements were obtained using the 514 nm laser with a motorized rotating λ/2 waveplate (30° steps), and a polarizer on the scattered beam as an

DOI: 10.1021/acsanm.9b02349
ACS Appl. Nano Mater. 2020, 3, 830−841

analyzer. The Raman Si peak, 3C-SiC TO peak, and the graphene[38] 2D to G peak intensity ratio were measured and plotted as a function of the angle (β) between the light polarization of the analyzer and the incident laser. Note that G peak has no polarization dependence due to the symmetry.[38] The graphene 2D peak is normalized to the G peak in order to minimize laser power fluctuations, as generally reported in the literature.[38]

X-ray Photoelectron Spectroscopy. X-ray photoelectron spectroscopy (XPS) measurements were performed using a Specs PHOIBOS 100 analyzer operated with a Mg Kα X-ray source (Mg anode operated at 10 keV and 10 mA) at 3 mm spot size. The data were calibrated to the C 1s peak present at 284.6 eV to compensate for any surface charging. The photoelectron peak areas were calculated after background correction by Shirley procedure.[41]

Density Functional Theory Calculations. All calculations were performed using the Quantum Espresso package.[69] At least 8 Å of vacuum space was included to decouple the structure from its periodic image. We used a 12 × 12 × 1 Monkhorst Pack grid to sample the Brillouin zone; refer to Sirikumara et al.[60] for more details on the calculations. In order to study the silicate layer of 3C-SiC, we used the model we proposed for oxidized 4H SiC(0001) surface, which was later used to study the epitaxial graphene on oxidized 4H-SiC(0001) surface.[60,70] The model has an R3 repeating cell of 3C-SiC (111) surface. Si_2O_3 ad-layer is chemically bound to 2 out of 3 surface Si atoms of the R3 cell via Si−O−Si bonds. Therefore, this model is also known as the Si_2O_5 model. In this work, we refer to this structure, Si_2O_5 on 3C-SiC(111), as an oxidized monolayer. Atomic configuration of 3C-SiC(111)/Si_2O_5 is fully optimized using the first-principles Density Functional Theory calculations. A 2 × 2 graphene cell is placed on the fully optimized R3 cell, and the geometry is again optimized.

H-Intercalation. H-intercalation is performed by annealing the EG/3C-SiC/Si sample in a Thermo Scientific Lindberg/Blue M Mini-Mite furnace in 1 atm of ultrapure hydrogen at 860 °C for 75 min. Similar conditions are also reported by Koch et al.[15] for quasi-freestanding bilayer epitaxial graphene on SiC(0001). The furnace was left to cool down at room temperature, and the sample was removed once the furnace reached room temperature.

■ ASSOCIATED CONTENT

Supporting Information

The Supporting Information is available free of charge at https://pubs.acs.org/doi/10.1021/acsanm.9b02349.

Additional figures, calculations, and analysis including Raman maps, Raman spectra, polar plots, EDX, XPS, sheet resistances, and DFT results (PDF)

■ AUTHOR INFORMATION

Corresponding Author

*E-mail: Francesca.iacopi@uts.edu.au.

ORCID

Aiswarya Pradeepkumar: 0000-0003-0669-5459
Mojtaba Amjadipour: 0000-0002-7938-7425
Neeraj Mishra: 0000-0003-3930-6210
Chang Liu: 0000-0002-0244-1999
Michael S. Fuhrer: 0000-0001-6183-2773
Avi Bendavid: 0000-0002-2454-9714
Fabio Isa: 0000-0002-1517-7242
Marcin Zielinski: 0000-0003-1663-3868
Hansika I. Sirikumara: 0000-0003-4625-755X
Thushari Jayasekara: 0000-0002-9556-8883
D. Kurt Gaskill: 0000-0001-7106-3605
Francesca Iacopi: 0000-0002-3196-0990

Author Contributions

The manuscript was written through the contributions of all authors.

Notes

The authors declare no competing financial interest.
[○]D. K. Gaskill has retired from US Naval Research Laboratory.

■ ACKNOWLEDGMENTS

Funding from the Air Force Office for Scientific Research through grants AOARD 17IOA027 and 18IOA052 is acknowledged. This work was performed in part at the Optofab and NSW nodes of the Australian National Fabrication Facility (ANFF). M. S. Fuhrer and C. Liu acknowledge support of the ARC Centre of Excellence in Future Low-Energy Electronics Technologies (CE170100039). The authors thank Mr. Geoff McCredie for his technical assistance in the UTS MAU laboratories. A. Bendavid and F. Isa acknowledge the support of the Melbourne Centre for Nanofabrication (MCN) in the Victorian node of the ANFF. Density Functional Theory calculations were done in the computer facilities provided by Southern Illinois University which were partly funded by National Science Foundation Awards 0721623 and 1032778.

■ REFERENCES

(1) Novoselov, K. S.; Geim, A. K.; Morozov, S. V.; Jiang, D.; Zhang, Y.; Dubonos, S. V.; Grigorieva, I. V.; Firsov, A. A. Electric Field Effect in Atomically Thin Carbon Films. *Science* **2004**, *306* (5696), 666−669.

(2) Ohta, T.; Bostwick, A.; Seyller, T.; Horn, K.; Rotenberg, E. Controlling the electronic structure of bilayer graphene. *Science* **2006**, *313* (5789), 951−954.

(3) Berger, C.; Song, Z.; Li, T.; Li, X.; Ogbazghi, A. Y.; Feng, R.; Dai, Z.; Marchenkov, A. N.; Conrad, E. H.; First, P. N. Ultrathin epitaxial graphite: 2D electron gas properties and a route toward graphene-based nanoelectronics. *J. Phys. Chem. B* **2004**, *108* (52), 19912−19916.

(4) De Heer, W. A. The invention of graphene electronics and the physics of epitaxial graphene on silicon carbide. *Phys. Scr.* **2012**, *T146*, 014004.

(5) De Heer, W. A.; Berger, C.; Wu, X.; First, P. N.; Conrad, E. H.; Li, X.; Li, T.; Sprinkle, M.; Hass, J.; Sadowski, M. L. Epitaxial graphene. *Solid State Commun.* **2007**, *143* (1−2), 92−100.

(6) Robinson, J. A.; Wetherington, M.; Tedesco, J. L.; Campbell, P. M.; Weng, X.; Stitt, J.; Fanton, M. A.; Frantz, E.; Snyder, D.; VanMil, B. L. Correlating Raman spectral signatures with carrier mobility in epitaxial graphene: a guide to achieving high mobility on the wafer scale. *Nano Lett.* **2009**, *9* (8), 2873−2876.

(7) Tedesco, J. L.; VanMil, B. L.; Myers-Ward, R. L.; McCrate, J. M.; Kitt, S. A.; Campbell, P. M.; Jernigan, G. G.; Culbertson, J. C.; Eddy, C. R., Jr; Gaskill, D. K. Hall effect mobility of epitaxial graphene grown on silicon carbide. *Appl. Phys. Lett.* **2009**, *95* (12), 122102.

(8) Lin, Y.-M.; Dimitrakopoulos, C.; Jenkins, K. A.; Farmer, D. B.; Chiu, H.-Y.; Grill, A.; Avouris, P. 100-GHz transistors from wafer-scale epitaxial graphene. *Science* **2010**, *327* (5966), 662−662.

(9) Escobedo-Cousin, E.; Vassilevski, K.; Hopf, T.; Wright, N.; O'Neill, A.; Horsfall, A.; Goss, J.; Cumpson, P. Local solid phase growth of few-layer graphene on silicon carbide from nickel silicide supersaturated with carbon. *J. Appl. Phys.* **2013**, *113* (11), 114309.

(10) Speck, F.; Jobst, J.; Fromm, F.; Ostler, M.; Waldmann, D.; Hundhausen, M.; Weber, H. B.; Seyller, T. The quasi-free-standing nature of graphene on H-saturated SiC (0001). *Appl. Phys. Lett.* **2011**, *99* (12), 122106.

(11) Norimatsu, W.; Kusunoki, M. Structural features of epitaxial graphene on SiC {0 0 0 1 surfaces. *J. Phys. D: Appl. Phys.* **2014**, *47* (9), 094017.

DOI: 10.1021/acsanm.9b02349
ACS Appl. Nano Mater. 2020, 3, 830−841

(12) Mammadov, S.; Ristein, J.; Koch, R. J.; Ostler, M.; Raidel, C.; Wanke, M.; Vasiliauskas, R.; Yakimova, R.; Seyller, T. Polarization doping of graphene on silicon carbide. *2D Mater.* **2014**, *1* (3), 035003.
(13) Kopylov, S.; Tzalenchuk, A.; Kubatkin, S.; Fal'ko, V. I. Charge transfer between epitaxial graphene and silicon carbide. *Appl. Phys. Lett.* **2010**, *97* (11), 112109.
(14) Daniels, K. M.; Jadidi, M. M.; Sushkov, A. B.; Nath, A.; Boyd, A. K.; Sridhara, K.; Drew, H. D.; Murphy, T. E.; Myers-Ward, R. L.; Gaskill, D. K. Narrow plasmon resonances enabled by quasi-freestanding bilayer epitaxial graphene. *2D Mater.* **2017**, *4* (2), 025034.
(15) Koch, R.; Fryska, S.; Ostler, M.; Endlich, M.; Speck, F.; Hänsel, T.; Schaefer, J.; Seyller, T. Robust phonon-plasmon coupling in quasifreestanding graphene on silicon carbide. *Phys. Rev. Lett.* **2016**, *116* (10), 106802.
(16) Dabrowski, J.; Lippert, G.; Avila, J.; Baringhaus, J.; Colambo, I.; Dedkov, Y. S.; Herziger, F.; Lupina, G.; Maultzsch, J.; Schaffus, T. Direct growth of low-doped graphene on Ge/Si (001) surfaces. 2016, arXiv:1604.02315. arXiv preprint archive. https://arxiv.org/abs/1604.02315.
(17) Lee, J.-H.; Lee, E. K.; Joo, W.-J.; Jang, Y.; Kim, B.-S.; Lim, J. Y.; Choi, S.-H.; Ahn, S. J.; Ahn, J. R.; Park, M.-H. Wafer-scale growth of single-crystal monolayer graphene on reusable hydrogen-terminated germanium. *Science* **2014**, *344* (6181), 286−289.
(18) Grzonka, J.; Pasternak, I.; Michałowski, P. P.; Kolkovsky, V.; Strupinski, W. Influence of hydrogen intercalation on graphene/Ge (0 0 1)/Si (0 0 1) interface. *Appl. Surf. Sci.* **2018**, *447*, 582−586.
(19) Portail, M.; Michon, A.; Vézian, S.; Lefebvre, D.; Chenot, S.; Roudon, E.; Zielinski, M.; Chassagne, T.; Tiberj, A.; Camassel, J. Growth mode and electric properties of graphene and graphitic phase grown by argon−propane assisted CVD on 3C−SiC/Si and 6H−SiC. *J. Cryst. Growth* **2012**, *349* (1), 27−35.
(20) Mishra, N.; Boeckl, J. J.; Tadich, A.; Jones, R. T.; Pigram, P. J.; Edmonds, M.; Fuhrer, M. S.; Nichols, B. M.; Iacopi, F. Solid source growth of graphene with Ni−Cu catalysts: towards high quality in situ graphene on silicon. *J. Phys. D: Appl. Phys.* **2017**, *50* (9), 095302.
(21) Ouerghi, A.; Marangolo, M.; Belkhou, R.; El Moussaoui, S.; Silly, M.; Eddrief, M.; Largeau, L.; Portail, M.; Fain, B.; Sirotti, F. Epitaxial graphene on 3C-SiC (111) pseudosubstrate: Structural and electronic properties. *Phys. Rev. B: Condens. Matter Mater. Phys.* **2010**, *82* (12), 125445.
(22) Moon, J.; Curtis, D.; Bui, S.; Marshall, T.; Wheeler, D.; Valles, I.; Kim, S.; Wang, E.; Weng, X.; Fanton, M. Top-gated graphene field-effect transistors using graphene on Si (111) wafers. *IEEE Electron Device Lett.* **2010**, *31* (11), 1193−1195.
(23) Kang, H.-C.; Karasawa, H.; Miyamoto, Y.; Handa, H.; Fukidome, H.; Suemitsu, T.; Suemitsu, M.; Otsuji, T. Epitaxial graphene top-gate FETs on silicon substrates. *Solid-State Electron.* **2010**, *54* (10), 1071−1075.
(24) Kang, H.-C.; Olac-vaw, R.; Karasawa, H.; Miyamoto, Y.; Handa, H.; Suemitsu, T.; Fukidome, H.; Suemitsu, M.; Otsuji, T. Extraction of drain current and effective mobility in epitaxial graphene channel field-effect transistors on SiC layer grown on silicon substrates. *Jpn. J. Appl. Phys.* **2010**, *49* (4S), 04DF17.
(25) Aristov, V. Y.; Urbanik, G.; Kummer, K.; Vyalikh, D. V.; Molodtsova, O. V.; Preobrajenski, A. B.; Zakharov, A. A.; Hess, C.; Hänke, T.; Büchner, B. Graphene synthesis on cubic SiC/Si wafers. Perspectives for mass production of graphene-based electronic devices. *Nano Lett.* **2010**, *10* (3), 992−995.
(26) Ouerghi, A.; Balan, A.; Castelli, C.; Picher, M.; Belkhou, R.; Eddrief, M.; Silly, M.; Marangolo, M.; Shukla, A.; Sirotti, F. Epitaxial graphene on single domain 3C-SiC (100) thin films grown on off-axis Si (100). *Appl. Phys. Lett.* **2012**, *101* (2), 021603.
(27) Gupta, B.; Notarianni, M.; Mishra, N.; Shafiei, M.; Iacopi, F.; Motta, N. Evolution of epitaxial graphene layers on 3C SiC/Si (1 1 1) as a function of annealing temperature in UHV. *Carbon* **2014**, *68*, 563−572.
(28) Ytterdal, T.; Cheng, Y.; Fjeldly, T. A. *Device modeling for analog and RF CMOS circuit design*; John Wiley & Sons, 2003.
(29) Aristov, V. Y.; Molodtsova, O. V.; Chaika, A. N. In *Growing graphene on semiconductors*; Motta, N., Iacopi, F., Coletti, C., Eds.; Pan Stanford, 2017; pp 27−75.
(30) Pradeepkumar, A.; Zielinski, M.; Bosi, M.; Verzellesi, G.; Gaskill, D. K.; Iacopi, F. Electrical leakage phenomenon in heteroepitaxial cubic silicon carbide on silicon. *J. Appl. Phys.* **2018**, *123* (21), 215103.
(31) Pradeepkumar, A.; Mishra, N.; Kermany, A. R.; Boeckl, J. J.; Hellerstedt, J.; Fuhrer, M. S.; Iacopi, F. Catastrophic degradation of the interface of epitaxial silicon carbide on silicon at high temperatures. *Appl. Phys. Lett.* **2016**, *109* (1), 011604.
(32) Suemitsu, M.; Miyamoto, Y.; Handa, H.; Konno, A. Graphene formation on a 3C-SiC (111) thin film grown on Si (110) substrate. *e-J. Surf. Sci. Nanotechnol.* **2009**, *7*, 311−313.
(33) Cançado, L.; Takai, K.; Enoki, T.; Endo, M.; Kim, Y.; Mizusaki, H.; Jorio, A.; Coelho, L.; Magalhaes-Paniago, R.; Pimenta, M. General equation for the determination of the crystallite size L a of nanographite by Raman spectroscopy. *Appl. Phys. Lett.* **2006**, *88* (16), 163106.
(34) Garlow, J. A.; Barrett, L. K.; Wu, L.; Kisslinger, K.; Zhu, Y.; Pulecio, J. F. Large-area growth of turbostratic graphene on Ni (111) via physical vapor deposition. *Sci. Rep.* **2016**, *6*, 19804.
(35) Malard, L.; Pimenta, M.; Dresselhaus, G.; Dresselhaus, M. Raman spectroscopy in graphene. *Phys. Rep.* **2009**, *473* (5−6), 51−87.
(36) Iacopi, F.; Walker, G.; Wang, L.; Malesys, L.; Ma, S.; Cunning, B. V.; Iacopi, A. Orientation-dependent stress relaxation in hetero-epitaxial 3C-SiC films. *Appl. Phys. Lett.* **2013**, *102* (1), 011908.
(37) Steele, J.; Puech, P.; Lewis, R. A. Polarized Raman backscattering selection rules for (hhl)-oriented diamond-and zincblende-type crystals. *J. Appl. Phys.* **2016**, *120* (5), 055701.
(38) Yoon, D.; Moon, H.; Son, Y.-W.; Samsonidze, G.; Park, B. H.; Kim, J. B.; Lee, Y.; Cheong, H. Strong polarization dependence of double-resonant Raman intensities in graphene. *Nano Lett.* **2008**, *8* (12), 4270−4274.
(39) Ramabadran, U.; Roughani, B. Intensity analysis of polarized Raman spectra for off axis single crystal silicon. *Mater. Sci. Eng., B* **2018**, *230*, 31−42.
(40) Hass, J.; Varchon, F.; Millán-Otoya, J.; Sprinkle, M.; de Heer, W.; Berger, C.; First, P.; Magaud, L.; Conrad, E. Rotational stacking and its electronic effects on graphene films grown on 4H-SiC(000$\bar{1}$). 2007, arXiv:0706.2134. arXiv preprint archive. https://arxiv.org/abs/0706.2134.
(41) Amjadipour, M.; Tadich, A.; Boeckl, J. J.; Lipton-Duffin, J.; MacLeod, J.; Iacopi, F.; Motta, N. Quasi free-standing epitaxial graphene fabrication on 3C−SiC/Si (111). *Nanotechnology* **2018**, *29* (14), 145601.
(42) Fukidome, H.; Kawai, Y.; Handa, H.; Hibino, H.; Miyashita, H.; Kotsugi, M.; Ohkochi, T.; Jung, M.-H.; Suemitsu, T.; Kinoshita, T. Site-selective epitaxy of graphene on Si wafers. *Proc. IEEE* **2013**, *101* (7), 1557−1566.
(43) Rollings, E.; Gweon, G.-H.; Zhou, S.; Mun, B.; McChesney, J.; Hussain, B.; Fedorov, A.; First, P.; De Heer, W.; Lanzara, A. Synthesis and characterization of atomically thin graphite films on a silicon carbide substrate. *J. Phys. Chem. Solids* **2006**, *67* (9−10), 2172−2177.
(44) Alves, D. C.; Silva, R.; Voiry, D.; Asefa, T.; Chhowalla, M. Copper nanoparticles stabilized by reduced graphene oxide for CO2 reduction reaction. *Materials for Renewable and Sustainable Energy* **2015**, *4* (1), 2.
(45) Biesinger, M. C.; Payne, B. P.; Grosvenor, A. P.; Lau, L. W.; Gerson, A. R.; Smart, R. S. C. Resolving surface chemical states in XPS analysis of first row transition metals, oxides and hydroxides: Cr, Mn, Fe, Co and Ni. *Appl. Surf. Sci.* **2011**, *257* (7), 2717−2730.
(46) Shinohara, M.; Yamanaka, M.; Daimon, H.; Sakuma, E.; Okumura, H.; Misawa, S.; Endo, K.; Yoshida, S. Growth of high-mobility 3C-SiC epilayers by chemical vapor deposition. *Jpn. J. Appl. Phys.* **1988**, *27* (3A), L434.

DOI: 10.1021/acsanm.9b02349
ACS Appl. Nano Mater. 2020, 3, 830−841

(47) Zhu, W.; Perebeinos, V.; Freitag, M.; Avouris, P. Carrier scattering, mobilities, and electrostatic potential in monolayer, bilayer, and trilayer graphene. *Phys. Rev. B: Condens. Matter Mater. Phys.* **2009**, *80* (23), 235402.
(48) Giesbers, A.; Procházka, P.; Flipse, C. Surface phonon scattering in epitaxial graphene on 6 H-SiC. *Phys. Rev. B: Condens. Matter Mater. Phys.* **2013**, *87* (19), 195405.
(49) Bryan, S. E.; Yang, Y.; Murali, R. Conductance of epitaxial graphene nanoribbons: Influence of size effects and substrate morphology. *J. Phys. Chem. C* **2011**, *115* (20), 10230−10235.
(50) Farmer, D. B.; Perebeinos, V.; Lin, Y.-M.; Dimitrakopoulos, C.; Avouris, P. Charge trapping and scattering in epitaxial graphene. *Phys. Rev. B: Condens. Matter Mater. Phys.* **2011**, *84* (20), 205417.
(51) Hwang, E.; Adam, S.; Sarma, S. D. Carrier transport in two-dimensional graphene layers. *Phys. Rev. Lett.* **2007**, *98* (18), 186806.
(52) Chen, J.-H.; Jang, C.; Adam, S.; Fuhrer, M.; Williams, E. D.; Ishigami, M. Charged-impurity scattering in graphene. *Nat. Phys.* **2008**, *4* (5), 377.
(53) Cavallo, F.; Rojas Delgado, R.; Kelly, M. M.; Sánchez Pérez, J. R.; Schroeder, D. P.; Xing, H. G.; Eriksson, M. A.; Lagally, M. G. Exceptional charge transport properties of graphene on germanium. *ACS Nano* **2014**, *8* (10), 10237−10245.
(54) Emtsev, K.; Speck, F.; Seyller, T.; Ley, L.; Riley, J. D. Interaction, growth, and ordering of epitaxial graphene on SiC {0001} surfaces: A comparative photoelectron spectroscopy study. *Phys. Rev. B: Condens. Matter Mater. Phys.* **2008**, *77* (15), 155303.
(55) Mishra, N.; Jiao, S.; Mondal, A.; Khan, Z.; Boeckl, J. J.; Gaskill, K. D.; Brock, R. E.; Dauskardt, R. H.; Iacopi, F. A graphene platform on silicon for the Internet of Everything. *2018 IEEE 2nd Electron Devices Technology and Manufacturing Conference (EDTM)* **2018**, 211−213.
(56) Kim, J.; Park, H.; Hannon, J. B.; Bedell, S. W.; Fogel, K.; Sadana, D. K.; Dimitrakopoulos, C. Layer-resolved graphene transfer via engineered strain layers. *Science* **2013**, *342* (6160), 833−836.
(57) Volinsky, A. A.; Moody, N. R.; Gerberich, W. W. Interfacial toughness measurements for thin films on substrates. *Acta Mater.* **2002**, *50* (3), 441−466.
(58) Wells, G.; Hopf, T.; Vassilevski, K.; Escobedo-Cousin, E.; Wright, N.; Horsfall, A.; Goss, J.; O'Neill, A.; Hunt, M. Determination of the adhesion energy of graphene on SiC (0001) via measurement of pleat defects. *Appl. Phys. Lett.* **2014**, *105* (19), 193109.
(59) Ristein, J.; Mammadov, S.; Seyller, T. Origin of doping in quasi-free-standing graphene on silicon carbide. *Phys. Rev. Lett.* **2012**, *108* (24), 246104.
(60) Sirikumara, H. I.; Jayasekera, T. Buffer-eliminated, charge-neutral epitaxial graphene on oxidized 4H-SiC (0001) surface. *J. Appl. Phys.* **2016**, *119* (21), 215305.
(61) Riedl, C.; Coletti, C.; Starke, U. Structural and electronic properties of epitaxial graphene on SiC (0 0 0 1): a review of growth, characterization, transfer doping and hydrogen intercalation. *J. Phys. D: Appl. Phys.* **2010**, *43* (37), 374009.
(62) Starke, U.; Riedl, C. Epitaxial graphene on SiC (0001) and: from surface reconstructions to carbon electronics. *J. Phys.: Condens. Matter* **2009**, *21* (13), 134016.
(63) Lauffer, P.; Emtsev, K.; Graupner, R.; Seyller, T.; Ley, L.; Reshanov, S.; Weber, H. Atomic and electronic structure of few-layer graphene on SiC (0001) studied with scanning tunneling microscopy and spectroscopy. *Phys. Rev. B: Condens. Matter Mater. Phys.* **2008**, *77* (15), 155426.
(64) Bekyarova, E.; Itkis, M. E.; Ramesh, P.; Berger, C.; Sprinkle, M.; de Heer, W. A.; Haddon, R. C. Chemical modification of epitaxial graphene: spontaneous grafting of aryl groups. *J. Am. Chem. Soc.* **2009**, *131* (4), 1336−1337.
(65) Ohta, T.; El Gabaly, F.; Bostwick, A.; McChesney, J. L.; Emtsev, K. V.; Schmid, A. K.; Seyller, T.; Horn, K.; Rotenberg, E. Morphology of graphene thin film growth on SiC (0001). *New J. Phys.* **2008**, *10* (2), 023034.
(66) Hass, J.; Feng, R.; Li, T.; Li, X.; Zong, Z.; De Heer, W.; First, P.; Conrad, E.; Jeffrey, C.; Berger, C. Highly ordered graphene for two dimensional electronics. *Appl. Phys. Lett.* **2006**, *89* (14), 143106.
(67) Kunc, J.; Hu, Y.; Palmer, J.; Guo, Z.; Hankinson, J.; Gamal, S. H.; Berger, C.; de Heer, W. A. Planar edge Schottky barrier-tunneling transistors using epitaxial graphene/SiC junctions. *Nano Lett.* **2014**, *14* (9), 5170−5175.
(68) Padilha, J.; Pontes, R.; de Lima, F. C.; Kagimura, R.; Miwa, R. Graphene on the oxidized SiC surface and the impact of the metal intercalation. *Carbon* **2019**, *145*, 603−613.
(69) Giannozzi, P.; Baroni, S.; Bonini, N.; Calandra, M.; Car, R.; Cavazzoni, C.; Ceresoli, D.; Chiarotti, G. L.; Cococcioni, M.; Dabo, I.; Dal Corso, A. QUANTUM ESPRESSO: a modular and open-source software project for quantum simulations of materials. *J. Phys.: Condens. Matter* **2009**, *21* (39), 395502.
(70) Starke, U.; Schardt, J.; Bernhardt, J.; Heinz, K. Reconstructed oxide structures stable in air: Silicate monolayers on hexagonal SiC surfaces. *J. Vac. Sci. Technol., A* **1999**, *17* (4), 1688−1692.

DOI: 10.1021/acsanm.9b02349
ACS Appl. Nano Mater. 2020, 3, 830−841